Journal of the European Ceramic Society 23 (2003) 1099–1104

www.elsevier.com/locate/jeurceramsoc

Improved high temperature properties of SiC-ceramics sintered with Lu_2O_3-containing additives

Koushik Biswas*, Georg Rixecker, Fritz Aldinger

Max-Planck Institut für Metallforschung and Institut für Nichtmetallische Anorganische Materialien, Universität Stuttgart, Pulvermetallurgisches Laboratorium, Heisenbergstraße 5, 70569 Stuttgart, Germany

Received 8 March 2002; received in revised form 8 July 2002; accepted 28 July 2002

Abstract

Liquid-phase (LPS) sintered silicon carbide ceramics with additive systems containing aluminium nitride and rare earth oxides in combination are candidate materials for good high temperature performance in terms of creep behaviour and oxidation resistance. In the present work, creep testing in four-point bending geometry and scanning electron microscopic observation of oxidized surfaces were performed on yttrium and lutetium sesquioxide containing materials, demonstrating that Lu_2O_3-containing sintering additives give rise to largely improved properties. In particular, strain rates of about 1×10^{-9} s^{-1} were measured at both 1400 °C/100 MPa and 1300 °C/300 MPa in air. Oxidation resistance of LPS-SiC sintered with Lu_2O_3 was measured in the temperature range 1200–1500 °C for 100 h and improved behaviour was observed as compared to other liquid phase sintered SiC with different additives.

Keywords: Creep; Oxidation; Rare earth oxides; SiC; Sintering

1. Introduction

Liquid phase sintered (LPS) silicon carbide is a candidate material for high temperature structural components. Sintering additives such as Al_2O_3–Y_2O_3 and AlN–Y_2O_3 were extensively used to obtain fracture resistant LPS-SiC ceramics.[1–9] Although numerous studies on silicon nitride, silicon carbide and sialons were carried out by using rare earth oxide-containing densification aids,[10–17] it was only recently that Lu_2O_3 was discovered to impart remarkably good high-temperature properties to Si_3N_4 ceramics.[18] This new rare earth sesquioxide additive systems were introduced for the modification of the grain boundaries and intergranular phases by highly refractory crystalline rare-earth disilicates leading to improved high temperature properties. In contrast, aluminium compounds as an ingredient of the sintering aid tend to compromise the high-temperature properties. This is because aluminium ions are able to act as network modifiers in siliceous glass,[19] decreasing its viscosity. However, aluminium compounds, to lower the eutectic temperature, cannot normally be avoided in LPS-SiC (as opposed to Si_3N_4 sintering) since rare earth oxides alone do not generate a sufficient amount of liquid phase at temperatures viable for sintering (<2100 °C). On the other hand, AlN is able to form forms a solid solution with SiC and thereby improves the high temperature properties as compared to the generic additive, Al_2O_3 [8]. Therefore, SiC sintered with Lu_2O_3–AlN additive is expected to be a good canditate for high temperature structural application. In the present paper, the relative merits of LPS-SiC materials with the additive systems AlN–Y_2O_3 and AlN–Lu_2O_3 are compared in terms of creep and oxidation resistance.

2. Experimental procedure

The starting materials used were commercially available α-SiC, β-SiC, AlN, Y_2O_3 and Lu_2O_3 powders. The characteristics of these powders are summarized in Table 1. Powder mixtures were prepared by attrition milling for 4 h in isopropanol, using Si_3N_4-balls with a ball-to-charge weight ratio of 6 to 1. After drying and

* Corresponding author.
E-mail address: biswas@aldix.mpi-stuttgart.mpg.de (K. Biswas).

0955-2219/03/$ - see front matter
PII: S0955-2219(02)00282-0

Table 1
Characteristics of the starting powders

Powder	Designation/ manufacturer	Chemical analysis [wt.%]	Particle size distribution			Specific area [m^2/g]	Density [g/cm^3]
			d_{10} [μm]	d_{50} [μm]	d_{90} [μm]		
α-SiC	A-10 H.C. Starck,Germany	C–30.0, O–0.9, Al–0.03, Ca–0.01, Fe–0.05	0.18	0.51	1.43	11.1	3.22
β-SiC	BF-12 H.C. Starck	C–30.0, O–1.2, Al–0.05, Ca–0.005, Fe–0.03	0.25	0.89	3.50	17.8	3.22
Y_2O_3	Grade C H.C. Starck	Al–0.005, Ca–0.003, Fe–0.005	1.21	4.48	8.08	12.9	5.02
AlN	Grade C H.C. Starck	N–30.0, C–0.1, O–2.5, Fe–0.005	0.34	0.92	3.07	5.0	3.26
Lu_2O_3	STREM, USA	Lu–99.9	–	–	–	–	9.45

granulation, by sieving with a mesh width of 160 μm, the processed powders were cold isostatically pressed at 240 MPa. The compositions of the powder premixes are given in Table 2.

Sintering was performed under N_2 atmosphere in a graphite-heated gas pressure furnace (Fine Ceramics Technologies, Germany), using heating rates of 20 °C/min to 1500 °C and 10 °C/min from 1500 °C to a sintering temperature of up to 2100 °C for the additive system 1Lu-1AlN. A nitrogen overpressure of 10 MPa was applied after 0.5 h at the sintering temperature. N_2 over pressure is applied in order to supress the decomposition reaction

$$2AlN \rightarrow 2Al\ (l) + N2\ (g)$$

at sintering temperature. The advantage of sintering in nitrogen over argon atmosphere was disscussed elsewhere [16].

Post-sintering annealing treatments were carried out at 1950 °C under N_2 at ambient pressure, using a graphite furnace (Astro Industries, USA). Further details on the techniques adopted for sintering can be found elsewhere [9].

Sintered densities were measured using Archimedes' water displacement method. Sintered and annealed samples were cut and ground to fine powder for qualitative phase analysis using X-ray diffraction (XRD, Siemens D 5000, filtered Cu K_α radiation). Specimen preparation for scanning electron microscopy (SEM) included a final polishing step with 1 μm diamond suspension and subsequent plasma etching in a O_2/CF_4 plasma (BioRad, Germany). A conventional SEM (S200, Cambridge Instruments, GB) equipped with an energy-dispersive spectrometer (EDS) was used for imaging and X-ray microprobe analysis. Carbon coating had to be applied at an acceleration voltage of 15 kV in order to avoid specimen charging effects.

Table 2
Compositions of powder premixes

Designation	SiC:additive [vol.%]	β-SiC:α-SiC [mol%]	Additive A:B [mol%]
1Lu–1AlN	90:10	90:10	50 Lu_2O_3:50 AlN
1Y–1AlN	90:10	90:10	50 Y_2O_3:50 AlN
3Y–2AlN	90:10	90:10	60 Y_2O_3:40 AlN

Four-point bend creep testing was performed in air on test specimens with dimensions 3 mm×4 mm×50 mm, using a universal testing machine (Zwick, Germany). The tensile surface of the bars was polished to a 3 μm diamond finish and the tensile edges beveled to avoid stress concentrations and large edge flaws caused by sectioning. The creep rate measurements are performed at temperatures of 1200, 1300, 1400, and 1500 °C with different applied stress levels varying from 50 to 300 MPa for a maximum duration of 60 h. The stress (σ_{4p}), calculated assuming elastic response to the imposed bending moment, is given by:[20]

$$\sigma_{4p} = \frac{3}{2}\cdot\frac{F(l_o - l_i)}{bh^2}, \quad (1)$$

where σ_{4p} = 4_point bending strength (MPa), F = force (N), l_o and l_i are the respective length between the two outer (40 mm) and inner supports (20 mm), b and h are breadth and height of the specimen, respectively. The strain (ε_{4p}) is calculated using the actual specimen displacement Δf relative to the inner load application points and can be expressed as:[21]

$$\varepsilon_{4p} = 4\cdot\frac{h\cdot\Delta f}{l_i^2}. \quad (2)$$

Oxidation experiments were conducted at different temperatures varying from 1200 to 1500 °C over a period of 100 h in air. Rectangular pellets (2 mm × 10 mm × 17 mm) are cut from the bulk specimen, ground and carefully mirror polished to 3 μm. The weight gain as a function of time is recorded by intermittently removing the specimens from the furnace after 1–36 h intervals for weighing and then putting them back.

3. Results and discussion

Relative densities in excess of 99% were achieved with all three additive systems. The SiC grains were equiaxed after sintering for 1 h, with plate-like morphologies evolving after prolonged annealing treatments of up to

60 h at 1950 °C (not shown here).[22] Phase analysis by XRD shows the existence of β-SiC and α-SiC along with silicon oxynitride and rare earth disilicates as minor phases. The grain boundary phases are mostly amorphous, with small amounts of crystalline phases at triple junctions.[22]

Fig. 1 shows the creep curve of different samples under 100 MPa stress at 1400 °C. It is obvious that the ceramic with the sintering additive Lu_2O_3–AlN has the lowest creep rate of all tested materials. Since annealing of material 3Y–2AlN (16 h at 1950 °C) decreases the creep rate substantially it is expected that 1Lu–1AlN will exhibit even lower creep rates after an appropriate heat treatment. Fig. 2 gives the temperature dependence of the strain rate at a constant stress of 300 MPa for SiC sintered with the Lu_2O_3–AlN additive.

The creep tests were analyzed by applying the Norton power-law relationship,

$$\dot{\varepsilon} = \mathrm{A}\cdot\sigma^{n}\cdot\mathrm{e}^{-Q/RT}, \tag{3}$$

where $\dot{\varepsilon}$ is the strain rate, A is a constant, σ is the creep stress, n is the steady state stress exponent, Q is the activation energy, R is the gas constant and T is the temperature in K. Since steady state creep was not reached after 60 h, stress exponents were calculated using the strain rates measured after $t = 20$ h. For different levels of stress and at different temperatures, creep parameters are determined from incremental stress or temperature changes using a general constitutive creep quation described in Eq. (3). Stress exponents, n, and activation energies, Q, are determined from the logarithmic plots strain rate ($\dot{\varepsilon}$) vs stress (σ), and $\log\dot{\varepsilon}$ vs. reciprocal of the temperature ($1/T$), respectively. The stress exponents were calculated to be 1.3–1.7 within the temperature range of 1300–1500 °C (Fig. 3). Apparent activation energies of 410, 310 and 400 kJ/mol were calculated for the stress levels of 100, 200 and 300 MPa, respectively (Fig. 4), which is in agreement with published values.[23,24]

The microstructure after creep testing is shown in Fig. 5. Due to the small total strain accumulated during testing (<0.5%) in bend geometry, there is no obvious

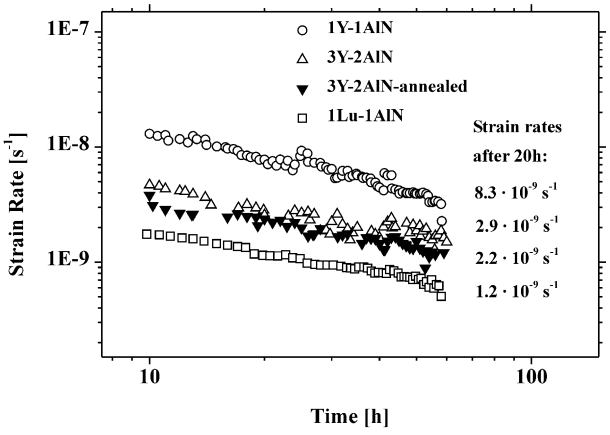

Fig. 1. Strain rate vs. time for different materials tested at 1400 °C in air, at a stress of 100 MPa.

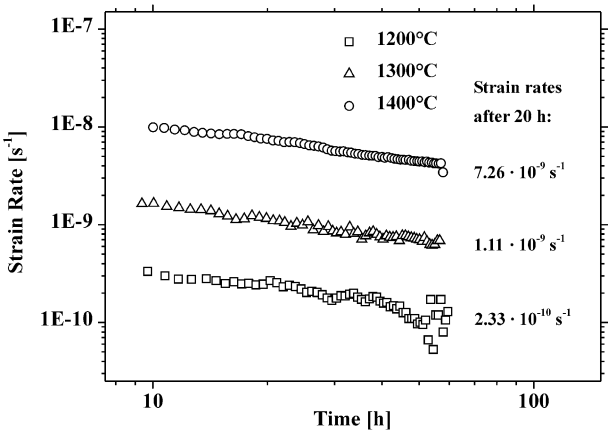

Fig. 2. Temperature dependence of the strain rate at 300 MPa for 1Lu–1AlN samples.

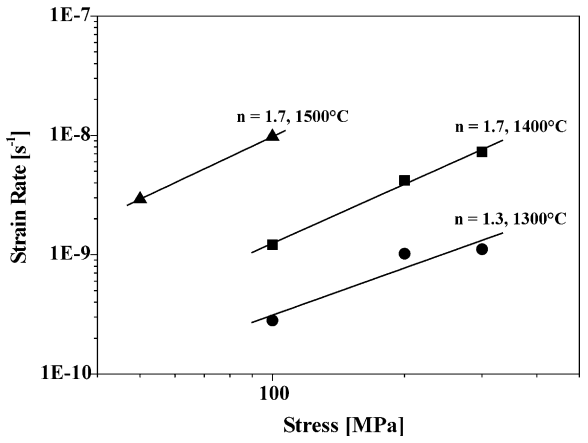

Fig. 3. Stress dependence of the strain rate for 1Lu–1AlN samples.

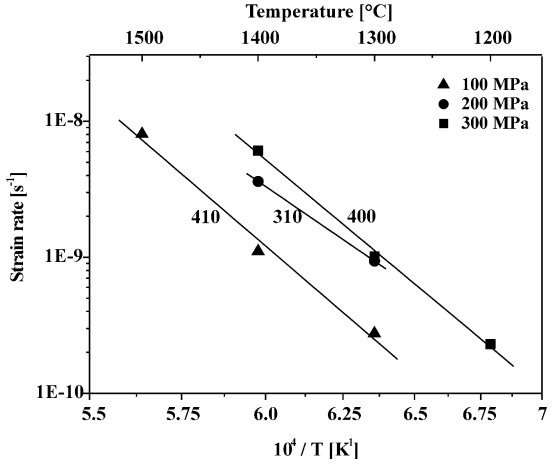

Fig. 4. Arrhenius plot of strain rates vs. reciprocal of temperature at different stress levels.

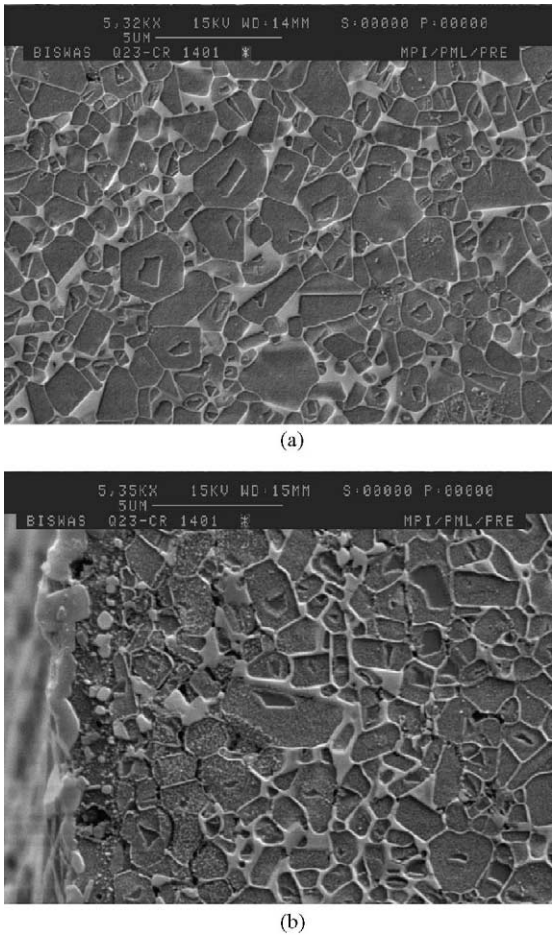

Fig. 5. Secondary electron images of 1Lu–1AlN samples after 60 h of creep deformation at 1400 °C/100 MPa: (a) bulk microstructure, (b) tensile surface.

change in the bulk microstructure (Fig. 5a). Some creep damage is visible underneath the tensile surface (Fig. 5b). However, creep cavitation damage and vaporization from the near-surface region of the samples may be superimposed, making it difficult to draw conclusions concerning the creep cavitation deformation mechanism from the microstructural observation.

Nagano et al.[25] found that flow stress dependency in compression and tension tests were almost same below the strain of 0.5%. So, main deformation mechanisms were thought to be the same in compression and in tension. In general, the linear flow stress dependency suggest the creep process is controlled by the diffusion process.[26] It is reported that viscous flow with a stress exponent $n=1$ is assumed to be probable deformation mechanism in an amorphous solid.[27] A somewhat higher stress exponent indicates that other mechanisms may also contribute to the deformation. Stress exponents of $n \sim 2$ suggest that bending creep is primarily influenced by interfacial reaction, intergranular glass phases, solution-reprecipitation, grain-boundary sliding and cavity formation.[24,25,28,32] Among these, microstructural evidence rules out the possibility of solution-reprecipitation during testing because there is no morphological change in the SiC-grains.

Activation energy is not considered as a sharp criterion for the creep mechanism, but comparison of the values can give some information about possible creep mechanisms. Activation energies (338–434 kJ/mol) were observed by Lane et al.[33] and Nixon et al.[34] in their respective studies with stress exponents of 1.4–1.7, which is well in accordance with the values obtained in this study. The creep mechanism in their studies is grain boundary sliding accomodated by grain boundary diffusion. The activation energies are very close to the activation energy for viscous flow of pure SiO_2 (≈440 kJ/mol).[35,36] Comparing the activation energies associated with creep deformation along with the stress exponent, the controlling creep mechanism in the present systems is supposed to be grain boundary sliding accomodated by diffusion along the grain boundary film/silicon carbide interface. A parallel mechanism, namely cavitation, may be operative above 1400 °C. However, from the microstructural observation, it is difficult to establish this fact due to the simultaneous occurrence of volatilization of the intergranular phase near the surface region.

Oxidation tests with 1Lu–1AlN samples were also conducted for 100 h at 1200, 1400 and 1500 °C in air. Fig. 4 shows the specific mass gain (mass gain per unit area) for specimens oxidized in air at temperatures between 1200 and 1500 °C. The oxidation kinetics are observed to be of the parabolic type, i.e. they are governed by the rate equation

$$\Delta W^2 = k_p\, t, \tag{4}$$

where ΔW is the weight gain per unit surface area, k_p is the rate constant of parabolic oxidation and t is the exposure time. The calculated parabolic rate constants are shown in Fig. 6. From the Arrhenius plot (Fig. 7),

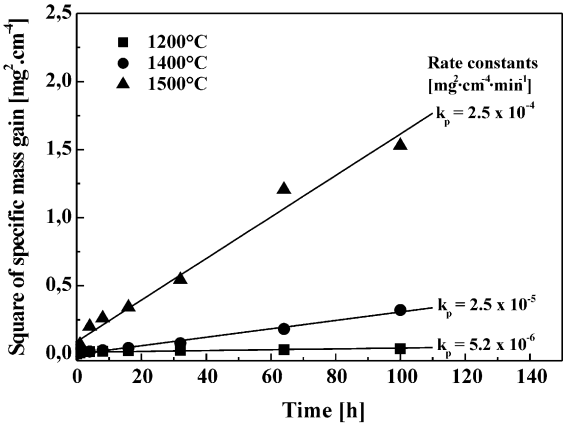

Fig. 6. Parabolic relationship between weight gain and time at different temperatures.

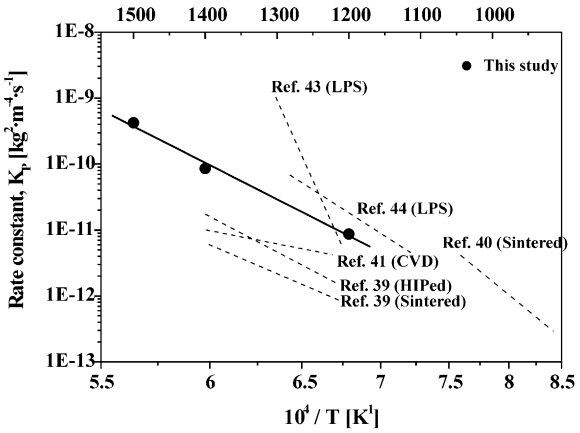

Fig. 7. A comparison of oxidation behaviour of this LPS-SiC (filled circles) with other different SiC (dashed line).

the activation energy between 1200 and 1500 °C is found to be 500±60 kJ mol^{-1}. It has been proposed that parabolic oxidation behaviour of ceramics indicates that the rate-determining step is a diffusional process associated with the migration of additive cations and anions along the secondary phases to the interface between the ceramic and the surface oxide.[10,37] A high activation energy, as it is found in the present study, suggests that oxidation proceeds not only by the diffusion of oxygen ion through the SiO_2 layer (Q_{ox} ~150 kJ mol^{-1}), but also by interfacial reactions between the growing SiO_2 layer and Lu_2O_3. So, oxidation is dominated by a surface or interface reaction controlled mechanism.[38]

A comparative plot of the oxidation kinetics (Fig. 7) shows that inspite of LPS-SiC, the oxidation behaviour is comparable with other silicon carbides, e.g. hot pressed with Al_2O_3 [39], solid-state sineterd with boron,[39,40] and CVD-SiC.[41] However, present material shows superior oxidation resistance to conventional liquid phase sintered SiC materials, particularly at higher temperatures—for comparison see, e.g. Refs. 42–44.

A tentative explanation for the superior creep and oxidation resistance would have to take into account anomalously strong bonding within the intergranular silicate phase, due to the small size of the Lu^{3+} cation, leading to high viscosity and reduced oxygen diffusivity. Another possibility would be reduced wetting between Lu_2O_3-rich liquid and SiC grains, as it was encountered in Lu_2O_3-doped Si_3N_4 ceramics.[18] In that study, however, stress exponents higher than 6 were measured in tensile creep, indicating that the creep mechanism was not a viscous flow of the grain boundary phase. SEM micrographs of the present material (Fig. 5a) do not provide any evidence for poor wetting between the silicon carbide grains and the intergranular phase.

4. Conclusions

Silicon carbide can be liquid phase sintered to theoretical density using the new additive system Lu_2O_3–AlN. Excellent creep resistance as well as oxidation resistance was obtained already for a material containing as much as 10 vol.% of this additive. Stress exponents and activation energies suggest that creep deformation is primarily controlled by grain boundary sliding accomodated by grain boundary diffusion. The parabolic oxidation behaviour shows that the kinetics of the oxidation process is complex and mainly controlled by surface reaction.

References

1. Padture, N. P. and Lawn, B. R., *J. Am. Ceram. Soc.*, 1992, **75**, 2518.
2. Mulla, M. A. and Kristic, V. D., *J. Mater. Sci.*, 1994, **29**, 934.
3. Padture, N. P., *J. Am. Ceram. Soc.*, 1994, **77**, 519.
4. Kim, Y.-W., Mitomo, M. and Hirotsuru, H., *J. Am. Ceram. Soc.*, 1995, **78**, 3145.
5. Keppeler, M., Reichert, H. G., Broadley, J. M., Thurn, G., Wiedmann, I. and Aldinger, F., *J. Eur. Ceram. Soc.*, 1998, **18**, 521.
6. Edington, J. W., Rowcliffe, D. J. and Hawshall, J. L., *Powder Metall. Int.*, 1975, **7**, 136.
7. Kodama, H. and Miyoshi, T., *J. Am. Ceram. Soc.*, 1992, **75**, 1558.
8. Lee, S. K. and Kim, C. H., *J. Am. Ceram. Soc.*, 1994, **77**, 1655.
9. Biswas, K., Rixecker, G., Wiedmann, I., Schweizer, M., Upadhyaya, G. S. and Aldinger, F., *Mater. Chem. Phys.*, 2001, **67**, 180.
10. Cinibulk, M. K. and Thomas, G., *J. Am. Ceram. Soc.*, 1992, **75**, 2037.
11. Goto, Y. and Thomas, G., *Acta Metall. Mater.*, 1995, **43**, 923.
12. Mandal, H., Camuscu, N. and Thompson, D. P., *J. Mater. Sci.*, 1995, **30**, 5901.
13. Choi, H. J., Lee, J. G. and Kim, Y.-W., *J. Mater. Sci.*,, 1997, **32**, 1937.
14. Bandyopadhyay, S., Hoffmann, M. J. and Petzow, G., *Ceram. Int.*, 1999, **25**, 207.
15. Choi, H. J., Lee, J. G. and Kim, Y. W., *J. Eur. Ceram. Soc.*, 1999, **19**, 2757.
16. Biswas, K., Rixecker, G. and Aldinger, F. *Proc. Materialsweek* (2000) Symp. I3. Available: http://www.materialsweek.org/proceedings/index.htm.
17. Kim, Y.-W., Mitomo, M. and Nishimura, T., *J. Am. Ceram. Soc.*, 2001, **84**, 2060.
18. Lofaj, F., Wiederhorn, S. M., Long, G. G., Jemian, P. R. and Ferber, M. K.. In *Ceramic Materials and Components for Engines*, ed. J. G. Heinrich and F. Aldinger. Wiley-VCH, Weinheim, 2000, pp. 487.
19. Rawson, H.. In *Materials Science and Technology,* Vol. 9, ed. R. W. Cahn, P. Haasen and E. J. Kramer. VCH, Weinheim, 1991, pp. 279.
20. Timoshenko, S.. In *Strength of Materials, Part II, Advanced Theory and Problems*, ed. S. Timoshenko. van Nostrand, Princeton, 1968.
21. Hollenberg, G. W., Terwillinger, G. R. and Gordon, R. S., *J. Am. Ceram. Soc.*, 1971, **54**, 196.
22. Biswas, K., Rixecker, G., Aldinger, F., submitted to CIMTEC 2002 conference, in press.
23. Gallardo-López, A., Muñoz, A., Martínez-Fernández, J. and Domínguez-Rodríguez, A., *Acta Mater.*, 1999, **47**, 2185.

24. Wiederhorn, S. M., Hockey, B. J. and French, J. D., *J. Eur. Ceram. Soc*., 1999, **19**, 2273.
25. Nagano, T., Kaneko, K., Zhan, G.-D., Mitomo, M. and Kim, Y.-W., *J. Eur. Ceram. Soc*., 2002, **22**, 263.
26. Dryden, J. R., Kucerovsky, D., Wilkinson, D. S. and Watt, D. F., *Acta Metall*., 1989, **37**, 2007.
27. Riedel, L., An, R., Konetschny, C., Kleebe, H.-J. and Raj, R. J., *Am. Ceram. Soc*., 1998, **81**, 1349.
28. Lin, M. T., Shi, J. L., Jiang, D. Y., Ruan, M. L. and Lai, T. R., *Mater. Sci. Eng., A*, 2001, **300**, 61.
29. Todd, J. A. and Zu, Z. Y., *J. Mater. Sci*., 1989, **24**, 4443.
30. Nagano, T., Kaneko, K., Zhan, G.-D. and Mitomo, M., *J. Am. Ceram. Soc*., 2000, **83**, 2497.
31. Wilkinson, D. S., *J. Am. Ceram. Soc*., 1998, **81**, 275.
32. Fields, B. A. and Wiederhorn, S. M., *J. Am. Ceram. Soc*., 1996, **79**, 977.
33. Lane, J. E., Carter, C. H. Jr. and Davis, R. F., *J. Am. Ceram. Soc*., 1988, **71**, 281.
34. Nixon, R. D., *R.F. Davis, J. Am. Ceram. Soc*., 1992, **75**, 1786.
35. Pezzotti, G., Kleebe, H.-J. and Ota, K., *J. Am. Ceram. Soc*., 1998, **81**, 3293.
36. Pezzotti, G., Kleebe, H.-J., Nishimura, H. and Ota, K., *J. Am. Ceram. Soc*., 2001, **84**, 2371.
37. Singhal, S. C., *J. Mater. Sci*., 1976, **11**, 500.
38. Harris, R. C. A., *J. Am. Ceram. Soc*., 1975, **58**, 7.
39. Costello, J. A. and Tressler, R. E., *J. Am. Ceram. Soc*., 1981, **64**, 327.
40. Luecke, W. E. and Kohlstedt, D. L., *J. Mater. Sci*., 1990, **25**, 5118.
41. Ogbuji, L. U. J. T. and Opila, E. J., *J. Electrochem. Soc*., 1995, **142**, 925.
42. Rixecker, G., Wiedmann, I., Rosinus, A. and Aldinger, F., *J. Eur. Ceram. Soc*., 2001, **21**, 1013.
43. Liu, D.-M., *Ceram. Int*., 1997, **23**, 425.
44. Jensen, R. P., Luecke, W. E., Padture, N. P. and Wiederhorn, S. M., *Mater. Sci. Eng*., 2000, **A282**, 109.